Self-compacting high-performance fiber concrete for foundations
Part 2—Fiber orientation and distribution

Grünewald, Steffen; Cotovanu, Bogdan; Rovers, John; Walraven, Joost; Taerwe, Luc

DOI
10.1002/suco.202000441

Publication date
2021

Document Version
Final published version

Published in
Structural Concrete

Received: 17 July 2020 | Revised: 19 October 2021 | Accepted: 3 December 2021

DOI: 10.1002/suco.202000441

ARTICLE

fib CEB-FIP WILEY

Self-compacting high performance fiber concrete for foundations: Part 2—Fiber orientation and distribution

Steffen Grünewald[1,2] | **Bogdan Cotovanu**[3] | **John Rovers**[3] | **Joost C. Walraven**[2,4] | **Luc Taerwe**[1,5]

[1]Department of Structural Engineering and Building Materials, Ghent University, Ghent, Belgium

[2]Department of Civil Engineering and Geosciences, Delft University of Technology, Delft, The Netherlands

[3]Shell Global Solutions, Rijswijk, The Netherlands

[4]College of Civil Engineering, Shenzhen University, Shenzhen, China

[5]College of Civil Engineering, Tongji University, Shanghai, China

Correspondence
Steffen Grünewald, Department of Civil Engineering and Geosciences, Delft University of Technology, Delft, The Netherlands.
Email: s.grunewald@tudelft.nl

Abstract

An investigation was executed into the applicability of self-compacting high performance fiber concrete in foundations. The applied concrete has a concrete cube strength of about 110 MPa and contains 60 kg/m^3 hooked-end steel fibers ($L_F = 30$ mm, $D_F = 0.38$ mm). This publication consists of two parts: (1) Experimental assessment and verification of design rules and (2) assessment of fiber orientation and distribution. In the first part, experiments are described which were carried out to determine the pre- and post-cracking strength properties, the shear resistance of short beams, the anchorage length of rebars, and the shear capacity of foundation slabs supported on piles. The test results were used for a verification and extension of design rules for fiber reinforced concrete (FRC) found in the *fib* Model Code 2010. The application of the FRC developed can lead to substantial savings in concrete and reinforcing steel. In the present second part, cross-sections of two slabs and a beam of this testing series have been analyzed with regard to fiber orientation and distribution. An image analysis, executed on 111 concrete areas, indicates that a preferred fiber orientation could not be identified throughout the assessed elements. The data supports the conclusion of a good fiber distribution as well; a strong correlation was obtained for the data set of full images between measured and theoretical relation of fiber orientation and fiber density.

KEYWORDS

fiber orientation, fiber reinforced concrete, image analysis, self-compacting concrete, steel fibers

1 | INTRODUCTION

In the first part of this two-part publication[1], it was shown that it is possible to produce a fiber reinforced concrete (FRC) in a strength class C80, which has strain-

Discussion on this paper must be submitted within two months of the print publication. The discussion will then be published in print, along with the authors' closure, if any, approximately nine months after the print publication.

hardening properties in uniaxial tension in spite of a fiber volume as low as 60 kg/m^3. This mixture was shown to be especially suitable for massive concrete elements like used for foundations. Moreover, this concrete is self-compacting, which further raises the attractivity for application in practice.

An important aspect of designing structures with self-compacting fiber reinforced concrete (SCFRC) is, however, the role of fiber orientation and distribution. fib Model Code 2010 already includes a concept to take these aspects into account.[2] In self-compacting concrete (SCC), fibers may be susceptible to orientation effects related to the flow direction. This implies uncertainties regarding the design strength values to be used. Cavalaro and Aguado[3] and Kooiman[4] concluded that results of tested small-scale laboratory specimens of FRC usually show a high scatter. In Part 1, it was already shown, that the load-crack mouth opening displacement (CMOD) curves, measured in 12 flexural standard tests on notched specimens, showed a relatively low coefficient of variation (COV) of only 14.2%, whereas this type of test is known for its large variation in results, because of its very small area, just above the notch, which governs the behavior. The variation also is determined by the mix design, the number of fibers and the consistency in procedure of filling molds when producing samples. In Grünewald[5], 17 series of flexural tests on SCFRC are reported where the flexural strength had a maximum variation of only 11.8% at the maximum based on three or four test specimens. Accordingly, the obtained result in this study is not uncommon and the low COV suggests already that the FRC used here has a low sensitivity for the effect of flow on fiber orientation and distribution. This could be an important conclusion, because it would mean that strength reduction factors for the post-cracking relations of this type of high performance fiber concrete (HPFC), intended to cope with a possible reducing effect of an unfavorable fiber orientation, would not be necessary.

This aspect was considered important enough to be further investigated on specimens used in the research described in Part 1. This concerns test specimens which were produced by a precast concrete company in Belgium and were tested in the Laboratory Magnel-Vandepitte of Ghent University in Belgium: three elements of those studies were selected for an assessment of fiber orientation and distribution by image analysis.

2 | FIBER DISTRIBUTION AND ORIENTATION

Fibers have been added as reinforcement of concrete and as such they are potentially able to (at least partially) replace traditional reinforcement like rebars or reinforcement meshes. Because of the specific characteristics of FRC special applications can be realized. In order to enhance the performance of structural concrete the homogeneity of fiber distribution and orientation have to be considered. Dependent on the matrix and fiber type, the pull-out performance of a fiber can either decrease or increase with a change of fiber inclination.[6,7] An increase of fiber pull-out resistance can be caused by additional frictional effects and mechanical deformation due to the bending of the fiber at the crack surface. Matrix spalling and fiber rupture can be the reason for a reduced overall fiber stress level.

With adequate mix design the fibers are well distributed in concrete after mixing and SCFRC is able to flow through the mold during casting. An important aspect to consider is that the fibers are not fixed by the matrix, but are rotating, if this movement is not counteracted by:

- Friction with aggregates or other fibers (to be minimized by adequate mix design);
- A clustering network of fibers (to be excluded by adequate mix design and fiber selection);
- A high yield stress and/or plastic viscosity of the SCC (to be affected by the mix design);
- Geometrical boundary conditions like formwork walls, reinforcement, previously cast concrete that has a too high yield stress for SCFRC to penetrate. The yield stress can increase after the flow has stopped due to thixotropic structural build-up of cement paste.[8]

Fibers remain in a stable position with regard to orientation when forced by the occurrence of locally high shear forces as in the case of a wall or a lower energy level (in the absence of walls, during free flow). Walls orient fibers parallel to its plane.[9] At increasing flow distance (distance between the location where the concrete is cast and the final location of the concrete in the mold), fibers can orient[5]; the effect of walls on fiber orientation was relatively more pronounced for longer steel fibers, indicating the geometrical interdependence between fiber length and their orientation. In the free-flow condition, fibers orient perpendicular to the flow direction of concrete.[5,10,11] The orientation of fibers can be influenced with a tailor-made casting process and in case, with the help of casting supporting tools.[12,13] However, HPFC can also be produced with a limited influence of the flow on fiber orientation, if a more random orientation is required, by limitation of the flow distance, as discussed in the next section.

3 | EXPERIMENTAL SET-UP

3.1 | Casting of prefabricated elements

The beams and slabs produced for the test series were casted with an approach that had to produce a fiber

orientation as close as possible to the random orientation. Details about the mix design are reported by Walraven et al.[1] As discussed, the flow of concrete can change the relative orientation of fibers. Accordingly, the flow distance had to be kept as short as possible. With regard to beam casting this means that the bucket has to move with the concrete front until the first layer of concrete is cast (Figure 1a). Casting progresses from one end to the other and back until the mold is filled. With this approach the flow distance is minimized. With the progress of casting, concrete can flow only when heights of concrete in the mold differ; a continuous movement along the beam prevents such differences. As a result, concrete is penetrating previously cast concrete at many locations and casting from a single location and longer flow distances are avoided.

In the first phase of slab filling, casting only from a single point has to be prevented, and filling of the mold best starts by casting along one wall of the mold (Figure 1b). Subsequently, concrete is cast just behind the casting front, which prevents the concrete behind from moving. Once the first layer is placed, casting proceeds in a continuous movement over the element. In contrast to beams, such movements occur in lanes besides each other to minimize height differences and the flow distance. With continuous vertical penetration of previously cast concrete potential preorientation due to the flow through the opening of the bucket also is reduced. The employees of the precast company were instructed in advance about the described casting approach.

3.2 | Selection of concrete elements for analysis

Two series of test specimens were produced with SCFRC by a precast concrete company in Belgium. The main target fiber contributions to the structural behavior were the transfer of shear forces, a better bond performance and a crack width reduction. As the main envisaged applications here are pile caps, in which a 3D force transfer occurs, any preferential fiber orientation has to be limited as much as possible. From the large number of test specimens, three FRC elements were selected for further analysis (a thick slab, a beam and a thin slab) with the aim to study the effect of the following aspects: type of element, location in element, distance from a wall and vertical and horizontal cutting. Table 1 provides an overview of the selected elements and cross-sections after sawing. The element type name refers to the element code of the prefabricated elements. Element 1 (Slab S) did not contain any rebar reinforcement, whereas reinforcement was present in Elements 2 and 3.[1] The areas for image analysis were chosen outside the area of reinforcement. The three elements (Nr. 1–3) were sawn in parts

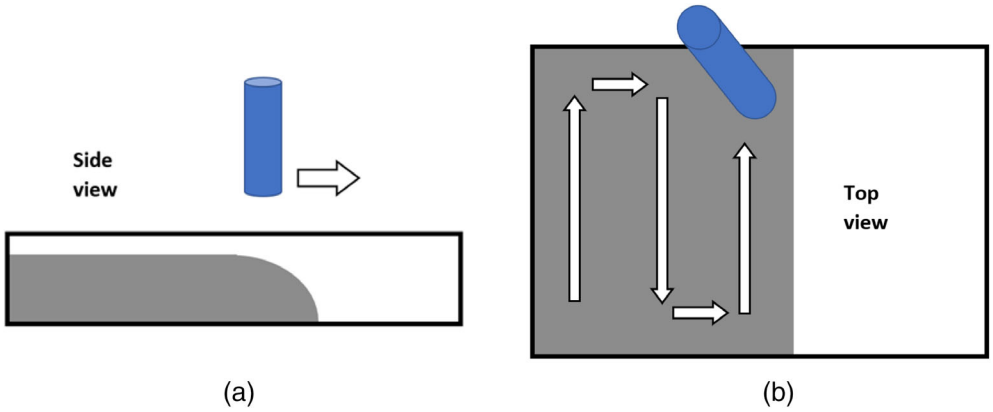

FIGURE 1 Two different casting methods for producing prefabricated elements in this study (a) beam casting and (b) slab casting

TABLE 1 Overview of elements and cross-sections selected for the image analysis

Element No.	Element type (dimensions in m)	Denotation of major cross-sections	Number of minor cross-sections	Cross-sectional area of minor cross-sections (mm × mm)
1	Slab S ($l_x = l_y = 2.5$ m, $h = 0.5$ m)	A, B, C	20	120 × 120
2	Beam type 1 ($l = 2.5$ m, $h = 0.5$ m, $b = 0.3$ m)	D, E, F	6	120 × 120
3	Slab type P ($l_x = l_y = 1.6$ m, $h = 0.3$ m)	G, H	11	100 × 100

along a number of planes, depending on the type of element (e.g., Element 1 was sawn along three major planes denoted as A, B, and C). Subsequently from those major planes minor areas were isolated by marking specific areas. In this way, altogether 37 minor areas were obtained which could be investigated with regard to fiber orientation and fiber density. Further details of the sawing process are given in the Sections 3.3 and 3.4 and Appendix.

3.3 | Cutting of elements and preparation of surfaces

A Dutch recycling company from Rotterdam got the task to arrange the sawing of the three selected elements, tested before at Ghent University, for the assessment of fiber orientation and distribution. Two methods were considered to cut the elements: (1) a water-cutting technique and (2) cutting with a diamond rope; the state of surface smoothness after cutting was not known beforehand. The water-cutting technique (high pressure water jet cutting) was tested first to cut the SCFRC-elements. The test was not successful, and the cutting was stopped, as the cutting front obviously was very rough. Next, a rope with a diamond-covered surface also was applied to separate the surfaces. Water was applied for cooling of the rope and to minimize the formation of dust. After cutting with the diamond rope a circular pattern was visible on all surfaces, which was the result of the rotating action of the cutting rope. After a first cleaning of the surface with water an initial test was executed to polish the surface with a small grinding machine. This grinding was insufficient to obtain a smooth surface. In a second step, the cross-sections had to be treated mechanically with a grinding wheel. The locations of the 37 minor cross-sections (Table 2 and Appendix) were measured in position and marked with a black marker. A considerable amount of material had to be removed from the concrete surface in order to obtain a sufficiently smooth and plain surface. Afterwards, the marked areas were polished with a grinding machine (paper fineness of 180) for about 20 s in order to obtain shining fiber surfaces which allowed taking photographs with a flashlight equipped camera. Finally, the elements were transported to the storage hall of the recycling company, in order to protect the steel fibers from corrosion due to contact with rainwater.

3.4 | Location of cut cross-sections

After cutting of the three elements in pieces, the 37 image cross-sections were measured in position. The positions of the different planes are specified in Table 2.

3.5 | Image analysis

In order to assure that all fibers receive a similar intensity of light for reflection, a diffuse state of light has to be provided with the flash of the camera. If the light is locally focussed, the difference in light intensity of the fibers in the pictures can be significant. Ideally, the light of the flash would come from behind (e.g., the flashlight of an umbrella-type of light-diffuser, which reflects the light in a diffuse manner back over the surface). It should be mentioned that not all fibers need to have a very bright color for the image analysis, as the applied image analysis software is able to recognize ranges of brightness (the threshold for brightness can be preselected). The following steps were executed:

- In order to increase the contrast of lightened fibers and the concrete the surface area was prewetted and just before taking the pictures it was dried with a towel to a surface-dry state;
- Pictures were taken from about a meter distance; the camera was zoomed in on the considered area;
- A strong external flashlight (not attached to the camera) was applied and positioned in front of the camera; in front of the flash a plain white paper was fixed to diffuse the light;
- After variation of several parameters like distance, prewetting and others, a good combination was obtained, and pictures of all 37 cross-sections were taken;
- Before proceeding to the next cross-section, the quality of the photograph of a cross-section was checked. Even with defined conditions, the quality of the pictures differed widely, with the distance and angle of the camera and flashlight with regard to the surface and the moisture condition of the surface being important parameters.

The software IMAGE J was applied for the analysis of the images of the minor cross-sections. The dimensions of the 37 (full) cross-sectional areas identified with a marker were measured with a ruler (accuracy: 1 mm); the number of fibers per image obtained from the image analysis was divided by the measured surface area of this cross-section. The outcomes of the analysis with IMAGE J were:

1. Areas of an image with a defined brightness (determined with a threshold, as shown by Figure 2) are identified;
2. Per identified area, the minimum and maximum diameters are obtained; the application of a cut-off criterion is required to identify fibers.

TABLE 2 Description of the locations and orientation of cut cross-sections of three elements

Element 1: Slab S (Series A, B, C) Cuts of Slab S, vertical cutting for planes A and B (see drawing), part C was cut in horizontal direction, the view on cross-sections of cutting planes A and B is from cut C. The Slab S failed during testing at Ghent University in the middle of the element with a crack plane parallel to the cutting line A. Planes A and B were obtained by vertical cutting (A was cut before B). Plane C was obtained by cutting the remaining concrete piece in two parts in horizontal direction (the bottom half of the element was assessed, 220 mm above the bottom of the element). The element cuts A and B were made at a distance of 700 mm from the side of the element.	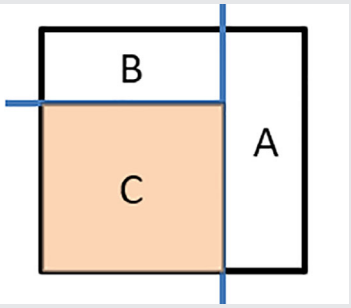 Slab S (top view)
Element 2: Beam type 1 (Series D, E, F) Series D, E, and F (2 images per vertical beam cut, cutting was executed in perpendicular direction to the longitudinal axis): the distances of the minor cross-sections from the bottom and walls of the element were 90 mm, from the top the distance was 80 mm. Series D: In the middle of the beam (distance from the end: 1.23 m), Series E: At 1/3 of the length of the beam (distance from the same end: 0.82 m) and Series F: At 1/6 of the length of the beam (distance from the same end: 0.41 m).	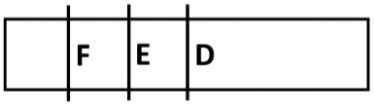 Beam type 1 (side view)
Element 3: Slab P (Series G, H) Cut G was carried out first, the distance from the side is 550 mm. Sufficient space was kept from the reinforcement in cut G in order not to observe steel in the image of cross-sections. The same 550 mm distance was kept from the side of the element for cut H. The location of the cross-sections in plane G also were selected not to cross reinforcement nor the crack running in a part of cut plane G.	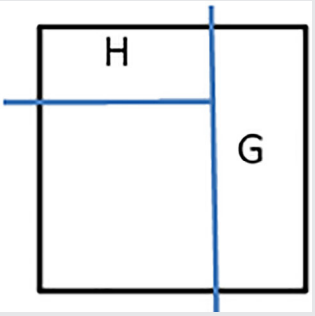 Slab P (top view)

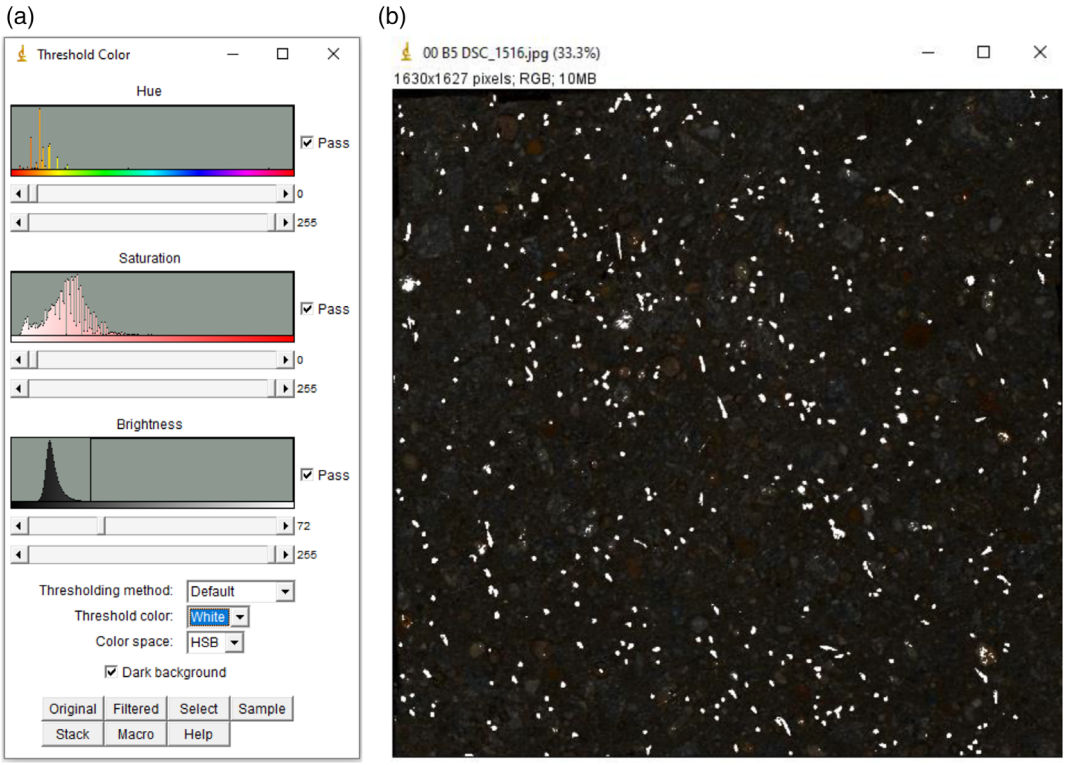

FIGURE 2 Example of an image analysis for Image B5 (a) threshold color selection settings and (b) 834 selected areas of which 607 were used for the analysis after the application of the cut-off criterion

The four steps of analysis with the software IMAGE J were:

- Selection of the complete image (in a pre-analysis step the pictures were rotated [if required] and trimmed to the dimensions between the lines drawn with the black marker);
- Enhancement of contrast;
- Threshold definition regarding brightness, as shown by Figure 2: the threshold value for brightness was altered until areas with bright colors in the concrete matrix reduced to very small separated areas;
- Analysis of particles (main outputs: minimum and maximum dimensions of identified areas).

The minimum dimension of a fiber's cross-section is the fiber diameter (minor axis of an ellipse); the maximum dimension is the major axis of the ellipse which is perpendicular to the minor axis. The main task of the analysis is to select only areas of bright spots that are fibers. The following approach was applied regarding the cut-off criterion:

- The average of the minimum diameters of all identified (remaining) areas was calculated (the minimum of a bright spot that is a fiber is its diameter). A threshold of ±30% (70–130% with regard to the average value) was chosen; areas below and above this threshold were removed from the data-set. This step was included to obtain a better estimation of the average minimum value. A larger number of small areas could influence the assumption that the average minimum area diameter is equal to the fiber diameter;
- A final threshold of 7.5% was applied to remove areas that do not have a minimum area diameter of 92.5–107.5% of the average minimum diameter of the, for the second time calculated, average minimum value (the calculated value is the average without the previously removed areas). With the chosen 7.5% criterion, the average of all cross-sections was 100% for the ratio experimental to theoretical fiber density (Table 3);
- After the two previous pre-selection steps, it is assumed that the remaining areas are fibers; the maximum dimension per area is the perpendicular diameter with which the fiber orientation can be calculated.

In order to further evaluate the variation of fiber orientation and fiber density within the 37 cross-sections, the following approach was applied. Black triangles were placed on the pictures, as can be seen in Figure 3. A triangle covers 50% of the area, which can be easily and accurately positioned from corner to corner and the remaining area is 50% of the total area of the picture. These pictures were saved as extra files and they were separately analyzed as discussed before, hereby 74 additional data-sets were obtained (111 images in total).

It should be mentioned that the image analysis is a tool with which fiber orientation and distribution of a cross-section can be determined. Limitations of the approach are:

- Influence of number of pixels: Figure 2 shows that Image B5 has an area of 1630 × 1627 pixels for a height and width of 121 and 122 mm (areas of other cross-sections: see Table 3), respectively. This translates to about 13.4 pixels/mm in height and width for this image. The fiber diameter is 0.38 mm, which is about 5.1 pixels for this minimum fiber dimension. Pixels cannot be divided, the maximum error can be as large as 1 pixel, which is about 20% of the fiber diameter.
- Fiber clustering: Fibers could be located in close vicinity of each other; when aligned in a row, this would result in a small under-estimation of the fiber orientation and fiber density. If the fibers would cluster in a circle, they would be removed due to the selected cut-off criterion.

3.6 | Calculation of the orientation number

The orientation number was determined according to Schönlin[14] with Equation (1).

$$\eta_{\varphi} = \frac{1}{N}\sum_{1}^{N} \cos\varphi \tag{1}$$

where N, number of fibers in the cross-section considered; φ, angle between considered plane and the steel fiber ($\cos\varphi = D_F/L_F$); D_F, diameter of steel fiber (mm); L_F, length of steel fiber in the cross-section (mm).

In the image assessment, cos φ is the ratio between the minimum and the maximum dimensions of an identified area. The orientation number is the average orientation of all remaining areas of the image analysis. A fiber orientation of 1 represents a spot, where the minimum and maximum dimensions are the same ($\cos\varphi = 1$), whereas with an orientation number close to zero a larger part of the cross-section of the fiber in length direction would be visible in the image. The fiber orientation is the highest (1.0) for aligned fibers in a single direction (1D); Schönlin[14] derived for the orientation in 2D and 3D orientation numbers of 0.785 and 0.66, respectively. To obtain a fiber orientation as close as possible to the random case of fiber orientation the described casting approach (Section 3.1) was selected.

TABLE 3 Results of the image analysis of 37 cross-sections

Nr.	Image code	Image nr.	Area (cm^2)	ON (–)	FN (–)	Thero. FD (Equation 2)	Exp. FD	((Theo.FD-Exp. FD) ^2)^0.5	Exp./Theor. FN (%)
1	A1	1410	145.2	0.75	861	5.09	5.93	0.84	117
2	A2	1434	142.8	0.69	700	4.63	4.90	0.28	106
3	A3	1448	145.2	0.81	616	5.45	4.24	1.21	78
4	A4	1449	145.2	0.83	847	5.60	5.83	0.23	104
5	A5	1455	144.0	0.77	740	5.19	5.14	0.05	99
6	A6	1461	145.2	0.55	375	3.72	2.58	1.14	69
7	A7	1472	145.2	0.67	733	4.52	5.05	0.53	112
8	A8	1478	142.8	0.61	600	4.15	4.20	0.06	101
9	B1	1480	145.2	0.61	653	4.10	4.50	0.39	110
10	B2	1482	146.4	0.57	726	3.83	4.96	1.13	130
11	B3	1484	146.4	0.66	794	4.45	5.42	0.97	122
12	B4	1507	145.2	0.68	645	4.56	4.44	0.12	97
13	B5	1516	147.6	0.63	607	4.25	4.11	0.14	97
14	B6	1522	146.4	0.41	470	2.76	3.21	0.45	116
15	C1	1539	144.0	0.58	634	3.93	4.40	0.47	112
16	C2	1545	144.0	0.72	826	4.84	5.74	0.89	118
17	C3	1579	148.8	0.73	629	4.91	4.23	0.68	86
18	C4	1589	148.8	0.74	821	4.99	5.52	0.53	111
19	C5	1592	146.4	0.46	507	3.08	3.46	0.38	112
20	C6	1599	145.2	0.52	535	3.51	3.68	0.17	105
21	D1	1613	147.6	0.74	551	5.01	3.73	1.28	74
22	D2	1624	146.4	0.70	802	4.71	5.48	0.77	116
23	E1	1629	144.0	0.77	625	5.18	4.34	0.84	84
24	E2	1661	147.6	0.69	726	4.66	4.92	0.26	106
25	F1	1666	146.4	0.73	730	4.94	4.99	0.04	101
26	F2	1677	147.6	0.66	619	4.48	4.19	0.29	94
27	G1	1721	100.0	0.71	396	4.76	3.96	0.80	83
28	G2	1726	100.0	0.68	475	4.58	4.75	0.17	104
29	G3	1741	102.0	0.55	413	3.72	4.05	0.33	109
30	G4	1749	101.0	0.61	368	4.11	3.64	0.46	89
31	G5	1753	100.0	0.68	452	4.57	4.52	0.05	99
32	G6	1754	99.0	0.61	391	4.09	3.95	0.14	97
33	G7	1767	100.0	0.61	363	4.13	3.63	0.50	88
34	G8	1775	103.0	0.83	461	5.60	4.48	1.12	80
35	H1	1691	98.0	0.71	462	4.79	4.71	0.08	98
36	H2	1699	98.0	0.66	389	4.46	3.97	0.49	89
37	H3	1715	98.0	0.74	476	5.00	4.86	0.14	97
Min				0.41			2.58	0.04	69
Max				0.83			5.93	1.28	130
Average				0.67			4.48	0.50	100

Abbreviations: FD, fiber density; FN, fiber number; ON, orientation number.

FIGURE 3 Preparation of additional pictures for the image analysis

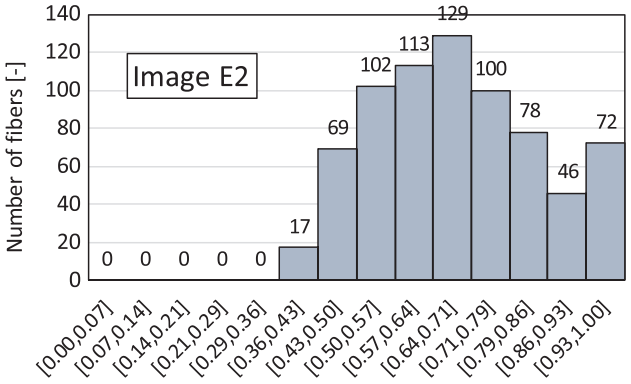

FIGURE 4 Histogram of frequency of fiber orientation for cross-section E2 (726 fibers in total)

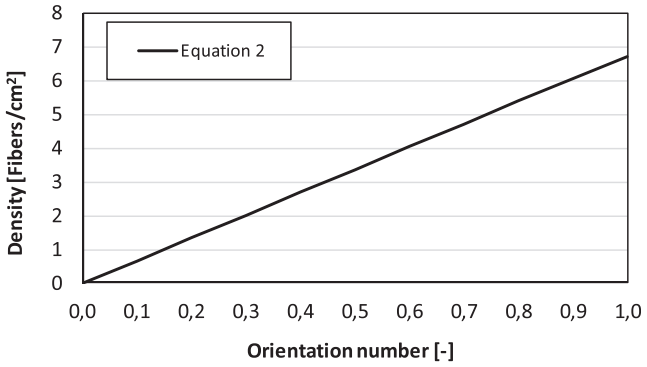

FIGURE 5 Theoretical fiber density dependent on the fiber orientation number (based on Equation 2, fiber dosage 60 kg/m^3, fiber diameter: 0.38 mm)

The orientation number determined with Equation (1) is an average number, which is distributed around an average value. Laranjeira de Oliveira[15] assessed results of an image analysis of cross-sections with regard to the distribution of fiber orientation and found that a good approximation is obtained with the Gaussian distribution which can be described by the average and a standard deviation, whereas Soetens[16] in some cases found a better fit of his results with other distribution functions. As an example, Figure 4 shows the frequency of occurrence of fiber orientation for Image E2 (average orientation number: 0.69). From the initial state of about random orientation in the mixer, fibers are in different states of rotation until the concrete hardens in the mold; the development in time of fiber orientation during mixing, transport, casting, and flow is reflected by the variation in fiber orientation.

The number of fibers visible in a cross-section depends on how fibers are oriented; the more inclined they are relative to the cracked surface, the relatively less fibers appear in the cross-section. The relationship is described by Equation (2).[17] The visible number of fibers depends on both the fiber orientation as well as on the volume of fibers in the concrete at this location (fiber distribution). Accordingly, the analysis of an image by only counting fibers does not provide sufficient information about fiber orientation. Often, a homogeneous fiber distribution is assumed throughout the concrete and the orientation number becomes the only unknown parameter. With an image analysis both the fiber number (fiber density) and their orientation can be independently determined. The fit between counted fiber number in the image with which the orientation number can be calculated with Equation (2) and the directly obtained fiber orientation (Equation 1) provides information regarding fiber distribution, as is discussed later in this article. The "fiber density" is the number of fibers N_F per area (Equation 2).

$$N_F = \frac{V_F}{A_F}\eta_\varphi \tag{2}$$

where N_F, fiber density: number of fibers (1/cm^2); V_F, fiber volume percentage; A_F, area of a single fiber (cm^2); and η_φ, orientation number in the direction perpendicular to the crack surface

Figure 5 shows for the applied steel fiber type ($L_f = 30$ mm; $D_f = 0.38$ mm; $V_f = 60$ kg/m^3) the relation between (average) fiber orientation and fiber density. The obtained linear line provides the theoretical values for

the comparison with values of fiber density versus fiber orientation obtained from the image analysis. In order to discuss fiber densities (not fiber volume), their orientation has to be known, which is a very important benefit of image analysis compared to other methods of fiber assessment (e.g., fiber counting method).

4 | RESULTS AND DISCUSSION

4.1 | Overview of results of the image analysis

In a first step, a total of 37 full cross-sections from different prefabricated elements, cut at different locations and in three directions were analyzed. The cross-sections were selected to represent the bulk volume of all produced elements. With this analysis approach the fiber distribution of prefabricated elements was assessed. Table 3 summarizes the important parameters and results of the image analysis. FN is the fiber number per image, ON is the dimensionless orientation number and FD is the fiber density in fibers per cm^2. The theoretical fiber density for the measured orientation number is calculated with Equation (2). The second last column lists the (positive) deviations between theoretical and experimental values of fiber density.

The average orientation number of all cross-sections was 0.67 on average, which is very close to the random number of 0.66 obtained by Schönlin,[14] the numbers were in the range of 0.41–0.83. The average deviation from the theoretical fiber density was 0.50 fibers/cm^2 and the range of deviations was 0.04–1.28 fibers/cm^2. With the total of all 37 cross-sections being 100% with regard to experimental divided by theoretical fiber densities (see also Section 3.5), the maximum and minimum values were 130% and 69%, respectively.

Figure 6 compares all results regarding orientation number and fiber density with the theoretical linear line derived from Equation (2). It should be mentioned that both the average orientation number and fiber densities are independently determined numbers obtained from the same image analysis (number of selected areas and assessment of areas' dimensions). The results are clearly correlated with the theoretical expected values. The results show the following:

- the relation between orientation number and fiber density holds true (the number of fibers of an area (fiber density) and orientation number are two independent results from the image analysis);
- the fibers are reasonably well distributed throughout the cross-sections (Table 3, last column compares theoretical and experimental fiber densities).

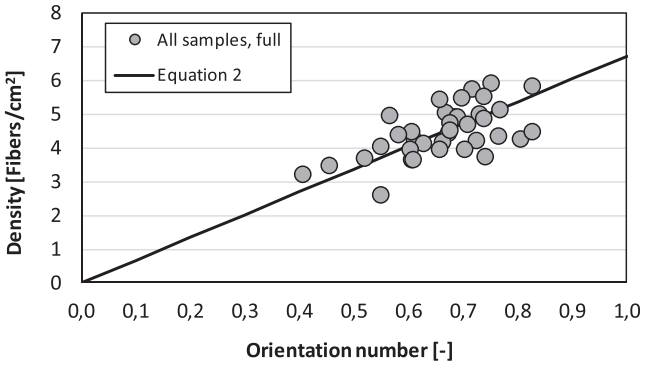

FIGURE 6 Theoretical and experimental orientation number vs fiber density (all full images)

In the following, the results of the image analyze are discussed in detail for the 37 full cross-sections of the three prefabricated elements.

4.2 | Results of Element 1 (slab with $h = 500$ mm)

Images of cross-sections of Series A–C (20 cross-sections) were obtained from Slab S. The planes A, B, and C of the element were a result of cutting in three different directions. Figure 7 summarizes the results for the Series A–C. The results fit well the theoretical correlation between fiber orientation and fiber density. A discussion of the statistical significance is included in Section 4.5. The average orientation number of Series A–C was on average 0.65 and with individual average values in the range of 0.41–0.83 (see also Table 3). The average deviation from the theoretical fiber density was 0.53 fibers/cm^2 and the range of deviation was 0.05–1.21 fibers/cm^2. With the total of all 20 cross-sections being in average 105% with regard to ratio experimental divided by theoretical fiber densities, the maximum and minimum values were 130% and 69%, respectively. The largest deviations (69% and 130%), with regard to the ratio experimental to theoretical fiber density were found in this slab.

Individual results are discussed in the following concerning the following aspects:

- Increase or decrease of orientation number and fiber density in a particular direction;
- Identification of the location of minimum or maximum values.

4.2.1 | Individual results Series A

The orientation numbers of the minor cross-sections of Series A are in three of four cases higher (more preferred

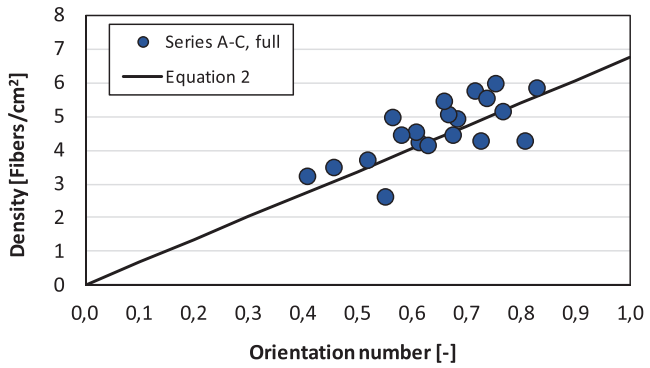

FIGURE 7 Average fiber orientations and fiber densities for Series A–C

A1 0.75 5.93 117%	**A3** 0.81 4.24 78%	**A5** 0.77 5.14 99%	**A7** 0.67 5.05 112%
A2 0.69 4.90 106%	**A4** 0.83 5.83 104%	**A6** 0.55 2.58 69%	**A8** 0.61 4.20 116%

FIGURE 8 Summary of experimental results for Series A (image code, average experimental orientation number [−], experimental fiber density [fibers/cm^2], experimental/theoretical fiber density [%])

orientation in the direction of the element cut) in the upper location of the element compared to the lower location (Figure 8). The higher orientation numbers can be the result of pre-orientation due to the flow through the bucket opening during casting. At the locations A4 and A6 the highest and lowest orientation numbers of plane A, respectively, were obtained with an orientation number of A4 being of the same order of magnitude as those of the upper locations' (A3) orientation number; the lower orientation number of A6 might be the result of the penetration of concrete in the concrete already being in the mold and the wall-effect of the bottom of the mold. The lowest ratio experimental to theoretical fiber density was obtained for cross-section A6 (69%), which is probably an area of turbulence where also fiber reorientation takes place (concrete was casted from above this location). Turbulence might also explain the somewhat lower fiber density since at a place of higher shear occurrence particle migration can take place within the concrete. Thrane et al.[18] also identified turbulent areas of reorientation through flow simulation for wall casting. An indication of turbulence in this area is also reflected by the relatively large difference in orientation numbers between A4 and A6. In a single case (A3 vs. A4), the relative ratio experimental to theoretical fiber densities was higher in the lower location, but fiber segregation could not be identified based on differences in fiber densities.

B1 0.61 4.50 110%	**B3** 0.66 5.42 122%	**B5** 0.63 4.11 97%
B2 0.57 4.96 130%	**B4** 0.68 4.44 97%	**B6** 0.41 3.21 101%

FIGURE 9 Summary of experimental results for Series B (image code, average experimental orientation number [−], experimental fiber density [fibers/cm^2], experimental/theoretical fiber density [%])

C6 0.52 3.68 105%	**C5** 0.46 3.46 112%	**C4** 0.74 5.52 111%
C1 0.58 4.40 112%	**C2** 0.72 5.74 118%	**C3** 0.73 4.23 86%

FIGURE 10 Summary of experimental results for Series C (image code, average experimental orientation number [−], experimental fiber density [fibers/cm^2], experimental/theoretical fiber density [%])

4.2.2 | Individual results Series B

The orientation numbers of the minor cross-sections of Series B are in the range of 0.41–0.68 (Figure 9). The difference with the results of Series A is obvious where orientation numbers obtained in the upper level mostly were higher (Figure 8). Probably, the difference is the consequence of how the casting bucket was oriented and moved over the formwork (see Section 3.1). With ratios experimental to theoretical fiber densities of about 100% or higher no fiber deficiency (area of lower fiber density in the upper cross-section) can be identified. The ratios of experimental to theoretical fiber densities were either higher or lower in the upper level and fiber segregation cannot be identified. As an overall conclusion on the results of Series A and B, fibers often are slightly more oriented in the plane parallel to the bottom of the mold (the orientation number is often higher than 0.66) and accordingly, lower orientation numbers can be expected in the third direction (which is perpendicular to plane C).

4.2.3 | Individual results Series C

The left side of Series C minor cross-sections (Figure 10) was in contact with the plane of Series B (see also Table 2 for a description). Cross-sections C5 and C6 were inside the element, whereas the other four cross-sections of plane C are located at 200 mm

distance from the vertical wall of the formwork. As discussed, a bit higher orientation numbers are obtained in the two planes which where vertically cut (Series A and B) and accordingly, relatively lower orientation numbers (less oriented in the direction perpendicular to plane C, which is upwards) are expected and observed for cross-sections C5 and C6.

4.3 | Results of Element 2 (beam with $h = 500$ mm)

A total of minor six cross-sections of a beam with a length of 2.5 m (Type 1) were assessed. The major cross-section D is located in the middle of the beam. The cross-sections E and F were located at a distance from the location of major cross-section D of 0.41 and 0.82 m, respectively. Figure 11 summarizes the results of Series D–F (the positions of the six minor cross-sections are shown in Figure 12). The results are in a smaller range of orientation numbers compared to the previously discussed Slab S, which reflects the lower degree of freedom of fibers to orient in a beam compared to a slab.

The average orientation number of Series D–F was 0.72 on average and the individual values being in the range of 0.66–0.77. The average deviation from the theoretical fiber density was 0.58 fibers/cm^2 (range: 0.04–1.28 fibers/cm^2).

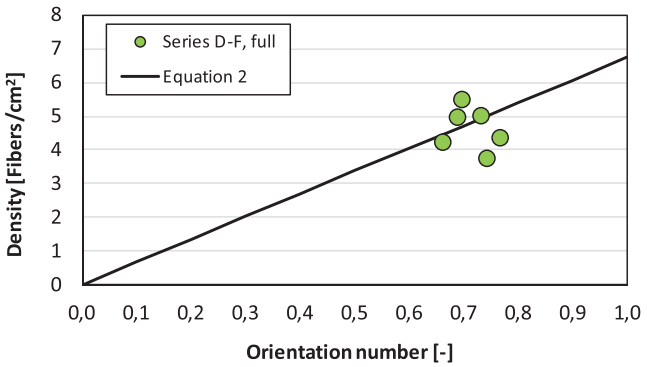

FIGURE 11 Average fiber orientations and fiber densities for Series D–F

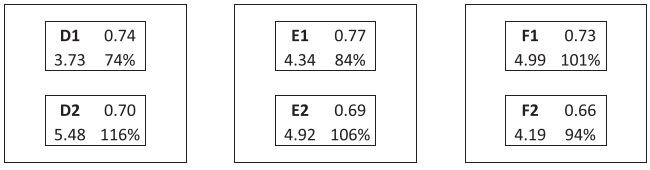

FIGURE 12 Summary of experimental results for Series D–F (image code, average experimental orientation number [−], experimental fiber density [fibers/cm^2], experimental/theoretical fiber density [%])

With the average of all six cross-sections being 96% with respect to the ratio experimental divided by theoretical fiber densities, the maximum and minimum values were 116% and 74%, respectively. The fiber volumes were comparable for the slab and the beam (average ratio experimental divided by theoretical fiber densities: 105% vs. 96%). No consistent change of orientation number in the length direction of the beam is observed, which allows to conclude that a preferred fiber orientation was not observed as the flow distance of the concrete during casting was kept short.

4.3.1 | Individual results Series D–F

The orientation numbers of the cross-sections of Series D–F are comparable (Figure 12). Like for the slab discussed before, the higher values were obtained more often for the upper level cross-sections. The flow through the casting bucket can influence fiber orientation, resulting in a bit higher values due to preorientation in flow direction during outflow. In the lower sections, the vertical wall of the formwork and the present reinforcement can reorient the fibers and hereby the average fiber orientation is reduced. As the orientation numbers of upper and lower sections are closer to each other in a beam compared to a slab, the effect of influencing boundary conditions seems to be more pronounced. The absolute value of fiber density differs between upper and lower minor cross-sections, but the trend is not consistent. The relative fiber volume (ratio experimental divided by theoretical fiber densities) of Series D is lower for the upper cross-section (D1) compared to the lower section (D2), which might indicate segregation of fibers or a more pronounced effect of turbulence. However, in the Series E and F, these values of upper and lower cross-sections are closer to 100% and each other.

4.4 | Results for Element 3 (slab with $h = 300$ mm)

A total of 11 minor cross-sections of a slab with a thickness of 300 mm were analyzed. The slab was cut in vertical direction and two perpendicular oriented planes were obtained. Figure 13 summarizes the results and they are in line with the results discussed in previous sections. A high correlation of experimental results with the theoretical line of Equation (2) is obtained; the result of cross-section G8 deviates more with the highest orientation number of this data-set. The average orientation number of Series G and H is 0.67 and the individual results are in the range of 0.55–0.83. The average deviation from the theoretical fiber density is 0.39 fibers/cm^2 (range: 0.05–1.12 fibers/cm^2). For the 11 minor cross-sections the ratio experimental to theoretical

fiber densities was 94% on average, with maximum and minimum values of 109% and 80%, respectively.

4.4.1 | Individual results Series G

Like in Series A and B, in Series G, a single lower value was obtained (G3: 0.55) reflecting the fact that this probably was a turbulence area from above which the concrete was cast (Figure 14). The penetration into the previously cast concrete occurs with turbulence which reorients the fibers. The thickness of both slabs differs (300 vs. 500 mm) and the assessed minor cross-sections of Series G are located closer to each other (20 vs. 100 mm of distance) in the thinner slab, as are the orientation numbers. In a thicker slab, casting takes place in more layers, which might be the reason why the preorientation (finishing casting action) is more prevalent in the upper level of the thicker slab. The orientation numbers in the upper level of cross-sections of the thinner slab are closer to the random orientation compared to the thicker slab. Segregation of fibers cannot be identified from the obtained data as the ratios experimental to theoretical fiber density in the lower level were inconsistently higher, about equal or lower. With average orientation numbers in a relatively narrow range, the fiber densities also were in a smaller range (3.63–4.75 fibers/cm^2).

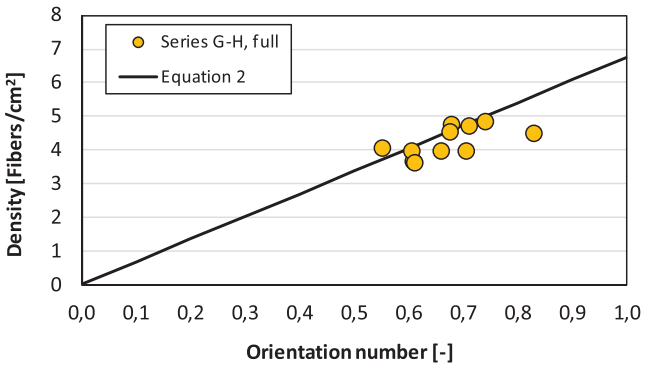

FIGURE 13 Average fiber orientations and fiber densities for Series G and H

G8	0.83	**G6**	0.61	**G4**	0.61	**G2**	0.68
4.48	80%	3.95	97%	3.64	89%	4.75	104%
G7	0.61	**G5**	0.68	**G3**	0.55	**G1**	0.71
3.63	88%	4.52	99%	4.05	109%	3.96	83%

FIGURE 14 Summary of experimental results for Series G (image code, average experimental orientation number [−], experimental fiber density [fibers/cm^2], experimental/theoretical fiber density [%])

4.4.2 | Individual results Series H

The right side of Figure 15 represents the side of plane H which was close to the cut plane of Series G. The fiber density and the ratio experimental to theoretical fiber densities of Series H are comparable with that of the neighboring areas in Series G (G3–G6); similar fiber densities were obtained for neighboring cross-sections H3, G4, and G6.

4.5 | Image analysis of half pictures

Figure 16 shows the results of fiber orientation and fiber density for all analyzed images separated for full and half areas. As the two halves together add up to a full picture, the average of the two halves is expected to be the outcome of the full image. The average deviation of the experimental and theoretical fiber densities of the 37 full images is 0.50 fibers/cm^2 (range: 0.04–1.28 fibers/cm^2), for the 74 half images it is a bit higher (0.58 fibers/cm^2, range: 0.01–1.87 fibers/cm^2).

The total amount of fibers of a full image is the sum of fibers of the two half images. The fiber numbers

		H1	0.71		
		4.71	98%		
				H3	0.74
				4.86	97%
H2	0.66				
3.97	89%				

FIGURE 15 Summary of experimental results for Series H (image code, average experimental orientation number [−], experimental fiber density [fibers/cm^2], experimental/theoretical fiber density [%])

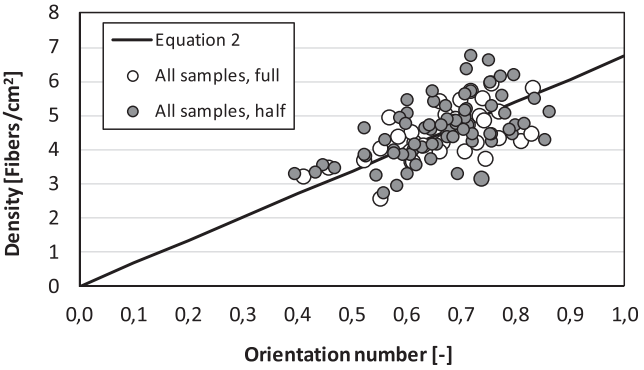

FIGURE 16 Overview of results of image analysis of 37 full images and 74 half images

were determined per half image and the lowest number was used to calculate the share of the total number per full image. Figure 17 shows this share of fiber number of the total fiber number for the 37 full images. 50% means that the fibers are evenly distributed over the two half cross-sections. It is obvious that in a smaller part of the full image a somewhat higher variation of fiber distribution is obtained and fibers are not equally distributed over the two halves of the cross-section. The individual results are in the range of 41.4–49.9% and the average deviation of two half images from 50% is 3.91%. With even smaller cross-sections the variation is expected to further increase.

Figure 17 shows that due to the division of the minor cross-sections (full image areas of 98–148 cm^2) also a somewhat larger variation of fiber distribution is obtained compared to the full image. Likewise, this can be expected for fiber orientation. Figure 18 shows the average fiber orientation numbers of half of the images (lower and higher average orientation number per full image); the average difference in fiber orientation between the two halves of the full images is 0.040 (range: 0.001–0.128).

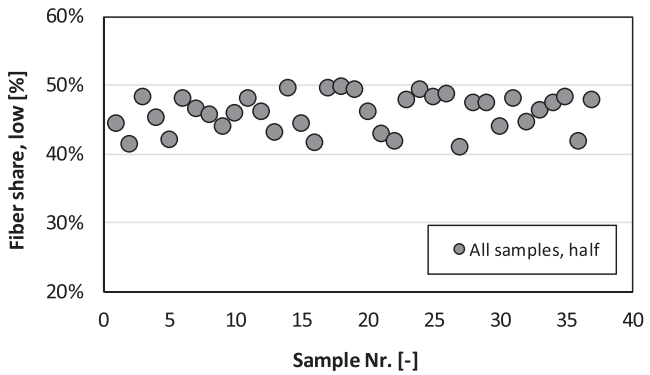

FIGURE 17 Minimum share of fibers in the two half images compared to the sum of fibers in both halves

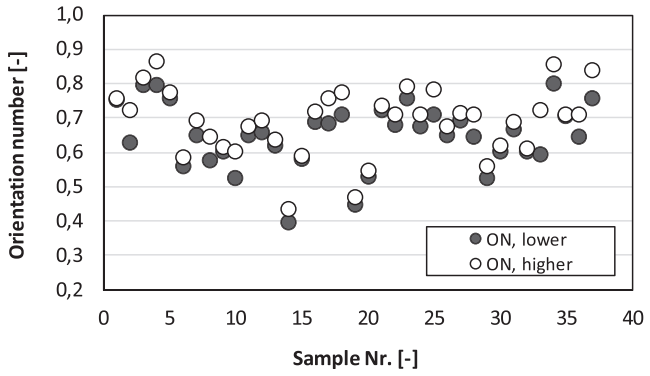

FIGURE 18 Lower and higher values of orientation number of the two halves of 37 full images

4.6 | Statistical significance

As Figure 6 and the previous discussion indicated, the experimental data points follow more or less the theoretical assumption expressed by Equation (2). In order to quantify the significance of the relation between the theoretical linear line and experimental data, both sets of full images as well as the pictures with half of the areas in black were analyzed to determine the coefficient of correlation. The correlation coefficient r is a numerical measure of correlation, meaning a statistical relationship between two variables. It indicates the strength and direction of the linear relationship and it is calculated by Equation (3). Values in the range from -1 to $+1$ can be obtained, where ± 1 indicate the strongest possible correlation and 0 the smallest possible correlation.[19]

$$r = \frac{\sum_{i=1}^{n}(x_i - \overline{x})(y_i - \overline{y})}{\sqrt{\sum_{i=1}^{n}(x_i - \overline{x})^2}\sqrt{\sum_{i=1}^{n}(y_i - \overline{y})^2}} \quad (3)$$

where n, number of variables; i, subscript; x, y, variables tested for correlation; and $\overline{x}, \overline{y}$, average value of x and y variables.

Table 4 summarizes the calculated correlation coefficients of the eight data-sets. Besides the complete data-sets of all full or half images, the same calculation was executed for both series for the large slab (A–C), the beam (D–H) and the small slab (G–H). The correlation coefficient is 0.61 for the complete data-set of full images, which is a strong correlation according to the scale of correlation coefficient ($0.60 \leq r < 0.80$).[20] The correlation coefficient obtained for Series A–C was 0.72, which is also a strong correlation. The correlation coefficients were -0.27 for Series D–H and 0.50 for Series G–H. Here, it should also be mentioned that the size of samples of Series G and H was smaller compared to the other series (sides of 100 mm vs. 120 mm), which can affect the outcome. Further, the lower correlation coefficient of Series D–F and G–H can be caused by the fact that the obtained range of orientation numbers was smaller, whereas the variation of the data-points from the average are comparable with the first two data-sets (all results & Series A–C). Furthermore, no directional effect was assessed in the beam (Series D–F); all cross-sections had the same orientation of their plane. Hereby, the difference between

TABLE 4 Correlation coefficients r for all series and different elements (full and half images), experimental and theoretical orientation number, and fiber density

Analysis	Series included	Type element	Sample number (–)	r, full image (–)	Sample number (–)	r, half image (–)
1	A–H	All	37	0.61	74	0.57
2	A–C	Slab, large	20	0.72	40	0.70
3	D–H	Beam, all	6	−0.27	12	−0.06
4	G–H	Slab, small	11	0.50	22	0.48

individual orientation number value and average orientation number as calculated with Equation (3) increases. This is also reflected by the higher deviation of data-points from the linear line of Equation (2) of half images compared to full images (Figure 16). Accordingly, the overall coefficients of correlation were a bit lower (all half images: correlation coefficient of 0.57), which is a moderate correlation coefficient ($0.40 \leq r < 0.60$).

The image analysis discussed in this article produced a satisfying result. For the consideration of the outcome, the reader should reflect on the following which can have an important effect:

- The study was executed with full-scale elements, not small scale laboratory samples. Cutting took place with a machine that has definitely a lower accuracy with regard to how flat the plane becomes compared to a saw;
- The image analysis was executed with specific assumptions (e.g., cut-off criteria) and the analysis very much depends on how many pixels are present in a picture. The applied fibers were very thin ($D_F = 0.38$ mm), and the smallest unit for the image assessment remains the pixel;
- The variation of FRC with regard to post-cracking performance depends on the location and orientation of the fibers which are affected by the size of the cross-section. The smaller the cross-section becomes the larger the variation is; this fact is known from studies varying for example the width of test specimens.[4] The sample size of the images evaluated in this study was relatively small compared to the elements from which they were extracted. According to the authors, further downscaling of images than done in this study would provide a wrong impression of variation in FRC and lacks relevance for the structural elements evaluated in this study. Nonetheless, such studies are valuable considering the performance of FRC on the fiber and FRC material levels;
- Finally, the mix design, the rheological properties and the execution of casting can also affect the local fiber density and orientation. For example, they can cause a local deviation of the fiber density compared to the expected value based on the calculation from the orientation number.

5 | CONCLUSIONS

This article discusses the distribution and orientation of steel fibers in prefabricated elements produced with High Performance Steel Fiber Reinforced Concrete. Three elements (two slabs and one beam) were selected for the analysis which were produced for and tested in two experimental series at Ghent University. The elements were cut at different locations and in different directions; cross-sections at different distances from the bottom of the prefabricated elements were also studied. A total of 111 images were assessed. Based on the study the following conclusions can be drawn:

- The number of fibers that crosses an area depends on the fiber orientation. The orientation numbers and fiber densities obtained by image analysis fit well the theoretically expected values, which is an indication of how the fibers are distributed throughout the elements. The deviation per assessed cross-section is discussed in this article;
- The deviation of fiber density compared to the theoretical value calculated based on the experimentally derived orientation number was at a maximum of 31% (cross-section A6) and 1.28 fibers/cm^2 in absolute terms (cross-section D1);
- The fiber distribution in three elements was assessed; segregation of fibers could not be identified based on the comparison of images at the bottom and the top of different locations;
- Important flow effects on fiber orientation were not observed, also not for the beam, for which a more

pronounced effect might be expected. The applied casting approach did not cause a preferred fiber orientation in the elements which is supported by the random nature of fiber orientation throughout the elements. The average of all average fiber orientation numbers is 0.67, with a range of 0.41–0.83.

- The flow through the casting bucket and its narrow opening probably preoriented the fibers. Through the penetration of the previously cast concrete, the presence of reinforcing bars and the walls of the formwork reorientation takes place; the degree of it also depends on the dimensions of the structural element and the casting approach;
- For the structural design of concrete structures with FRC the variation of material characteristics, the orientation of fibers and the size of the structure need to be considered. This is already foreseen for example in the concept of the new Eurocode 2 where FRC is included in Annex L. This article discussed these aspects in more detail. The research shows that with a well-composed concrete and an optimized casting procedure the assumed effect of fiber orientation can be compensated for. Such information should be included as information and comment in future recommendations. The variation of material characteristics is not an intrinsic property of FRC, but it is also determined by aspects like mix design or filling procedure of test specimens.

DATA AVAILABILITY STATEMENT

Data available on request from the authors

ORCID

Joost C. Walraven https://orcid.org/0000-0003-3243-8878

REFERENCES

1. Walraven JC, Droogné D, Grünewald S, Taerwe L, Cotovanu B, Rovers J. Self-compacting high-performance fiber concrete for foundations: part 1—experimental verification and design considerations. fib Struct J. 2021;51:1–15. https://doi.org/10.1002/suco.202000440
2. fib Model Code 2010 (2013), *fib* model code for concrete structures 2010, Wilhelm Ernst & Sohn.
3. Cavalaro SHP, Aguado A. Intrinsic scatter of FRC: an alternative philosophy to estimate characteristic values. Mater Struct. 2015;48:3537–55. https://doi.org/10.1617/s11527-014-0420-6
4. Kooiman, A.G. (2000), Modelling steel fibre reinforced concrete for structural design, PhD Thesis, Department of Structural and Building Engineering, Delft University of Technology.
5. Grünewald, S (2004), Performance-based design of self-compacting fibre reinforced concrete, PhD Thesis, Delft University of Technology.
6. Robins P, Austin S, Jones P. Pull-out behaviour of hooked steel fibres. Mater Struct. 2002;35(8):434–42.
7. Van Gysel, A (2000), Studie van het uittrekgedrag van staalvezels ingebed in een cementgebonden matrix met toepassing op staalvezelbeton onderworpen aan buiging, PhD Thesis, Ghent University. (in Dutch)
8. Roussel N, Ovarlez G, Garrault S, Brumaud C. The origins of thixotropy of fresh cement pastes. Cem Concr Res. 2012;42(1):148–57.
9. Martinie L, Roussel N. Simple tools for fiber orientation prediction in industrial practice. Cem Concr Res. 2011;41:993–1000.
10. Abrishambaf A, Barros JAO, Cunha VMCF. Relation between fibre distribution and post-cracking behaviour in steel fibre reinforced self-compacting concrete panels. Cem Concr Res. 2013;51:57–66.
11. Žirgulis, G (2015), Fibre orientation in steel-fibre-reinforced concrete, PhD thesis NTNU Trondheim.
12. Ferrara, L, Cremonesi, M. (2013), Effects of casting process on toughness properties of fiber reinforced-self compacting concrete as from EN 14651. Paper presented at Proceedings of 7th RILEM International Conference on SCC, Roussel, N.; Bessaies-Bey, H. (Eds.), Paris, RILEM Publications S.A.R.L., Bagneux.
13. Grünewald, S, Bartoli, L, Ferrara, L, Kanstad, T, Dehn, F (2016), Translation of test results of small specimens of flowable fibre concrete to structural behaviour: A discussion paper of fib Task Group 4.3, fib Bulletin No. 79, Proceedings of the FRC 2014 ACI-fib International Workshop Fibre-Reinforced Concrete: From design to structural applications, pp. 81–90.
14. Schönlin K. Determination of the orientation, the content and the distribution of the fibres in fibre reinforced concrete. Beton- und Stahlbetonbau. 1988;83(6):168–71. (in German).
15. Laranjeira de Oliveira, F (2010), Design-oriented constitutive model for steel fiber reinforced concrete, PhD Thesis, Universitat Politècnica de Catalunya, Barcelona.
16. Soetens, T (2015), Design models for the shear strength of Prestressed precast steel fibre reinforced concrete girders, PhD Thesis. Ghent University
17. Stang H, Li V. Mechanics of fiber reinforced cement based composites, course material—International Graduate. Lyngby: Research School in Applied Mechanics; 2001.
18. Thrane LN, Svec O, Strøm M, Kasper T. Guideline for execution of steel fibre reinforced SCC. Printing, Paritas A/S, Taastrup/Denmark: Danish Technological Institute; 2013.
19. Taylor JR. An introduction to error analysis, the study of uncertainties in physical measurements. 2nd ed. Sausalito/USA: University Science Books; 1997.
20. Web Search (2021), 29-09-2021, www.bing.com/images/search?view=detailV2&ccid=gPmFwhE7&id=135A18E275BD318092FB9499DEC952A964B2B1B7&thid=OIP.gPmFwhE79F5ZCf1WAaxI4QHaEp&mediaurl=https%3a%2f%2fspencermath.weebly.com%2fuploads%2f2%2f0%2f8%2f8%2f20886508%2f9242673_orig.png&cdnurl=https%3a%2f%2fth.bing.com%2fth%2fid%2fR.80f985c2113bf45e5909fd5601ac48e1%3frik%3dt7GyZKlSyd6ZlA%26pid%3dImgRaw%26r%3d0&exph=541&expw=863&q=interpret+correlation+coefficient&simid=608002171940063275&FORM=IRPRST&ck=12EC28B284232F70A4358D064E6FE631&selectedIndex=0&idpp=overlayview&ajaxhist=0&ajaxserp=0

AUTHOR BIOGRAPHIES

Steffen Grünewald, Faculty of Civil Engineering, Delft University of Technology, Delft, The Netherlands; Department of Structural Engineering and Building Materials, Ghent University, Ghent, Belgium
s.grunewald@tudelft.nl

Bogdan Cotovanu, Shell Global Solutions, Rijswijk, The Netherlands
bogdan.cotovanu@shell.com

John Rovers, Shell Global Solutions, Rijswijk, The Netherlands
john.rovers@shell.com

Joost C. Walraven, Faculty of Civil Engineering, Delft University of Technology, Delft, The Netherlands; College of Civil Engineering, Shenzhen University, Shenzhen, China
jcwalraven@hotmail.com

Luc Taerwe, Department of Structural Engineering and Building Materials, Ghent University, Ghent, Belgium; Tongji University, College of Civil Engineering, Shanghai, China
luc.taerwe@ugent.be

How to cite this article: Grünewald S, Cotovanu B, Rovers J, Walraven JC, Taerwe L. Self-compacting high performance fiber concrete for foundations: Part 2—Fiber orientation and distribution. Structural Concrete. 2022;1–18. https://doi.org/10.1002/suco.202000441

APPENDIX

Locations of cross-sections for image analysis

⇒ Series A (dimensions: 2.5 × 0.7 × 0.5 m^3): eight cross-sections, the distances of the cross-sections from the sides were 100 mm from the wall (left and right) and bottom, 80 mm from the top of the element, the distance between cross-sections A1 (A2) and A3 (A4) as well as A5 (A6) to A7 (A8) was 600 mm (Figure A1).

⇒ Series B (dimensions: 1.2 × 0.7 × 0.5 m^3): six cross-sections (Figure A2), the distance from the sides were: 100 mm from the wall, 80 mm from the top and bottom of the element, the distance between cross-sections in horizontal direction was 190 mm. The right side of plane B is a part of the cracked side of Slab S3.

⇒ Series C (dimensions: 1.79 × 1.25 × 0.22 m^3): six cross-sections, the distance from the sides were (C1–C6 were marked counter-clockwise): 200 mm from the wall and cut plane B, the distances in between C1, C2, and C3 (and also between C4, C5, and C6) were 510 mm. The distance in the perpendicular direction between the different locations was

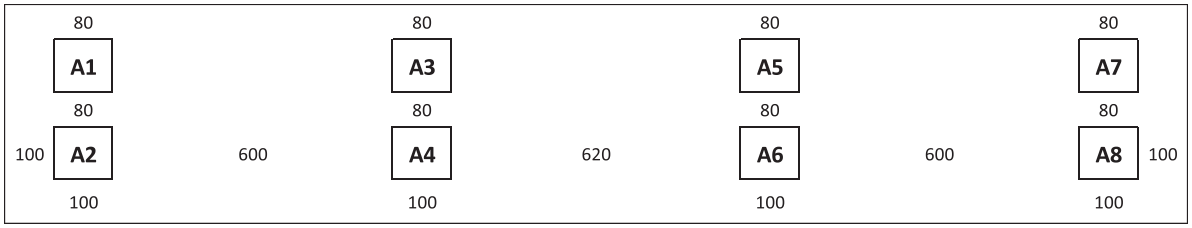

FIGURE A1 Location of cross-sections of Series A (8 cross-sections, size: 120 × 120 mm^2)

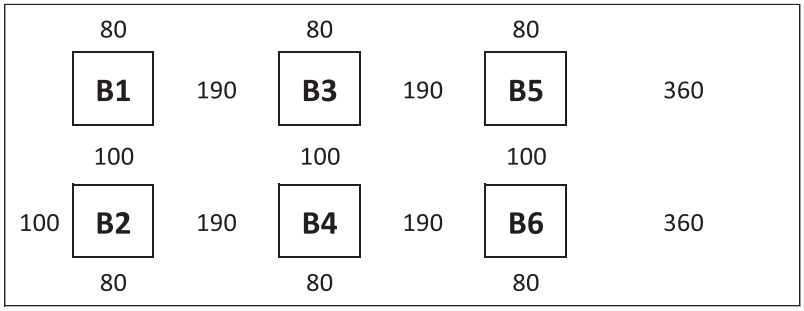

FIGURE A2 Location of cross-sections of Series B (6 cross-sections, size: 120 × 120 mm^2)

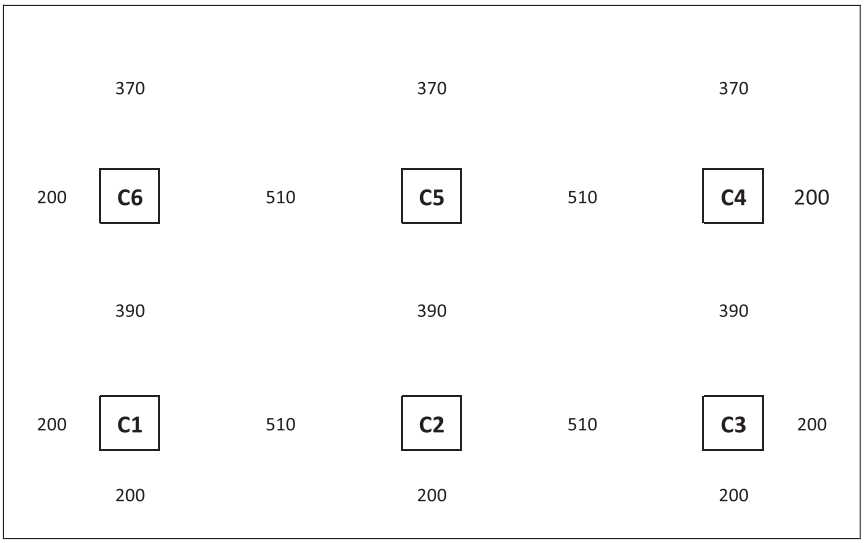

FIGURE A3 Location of cross-sections of Series C (6 cross-sections, size: 120 × 120 mm^2)

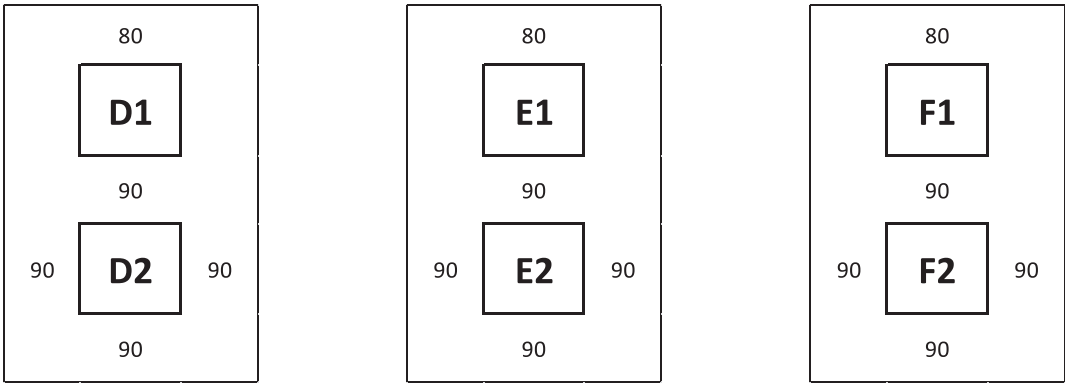

FIGURE A4 Overview of the cross-sections of Series D–F (Beam type 1), dimensions cross-section of beam: 0.5 × 0.3 m^2

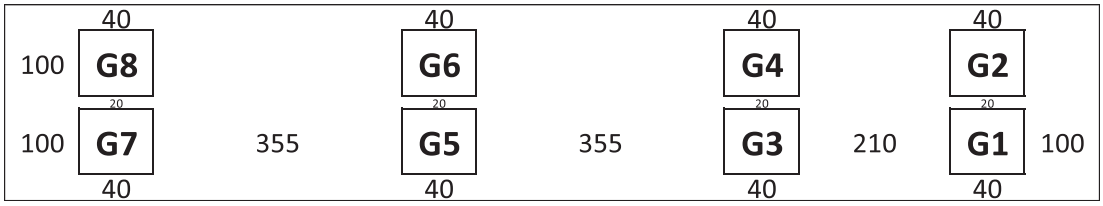

FIGURE A5 Location and coding of cross-sections of Series G (8 cross-sections, size: 100 × 100 mm^2)

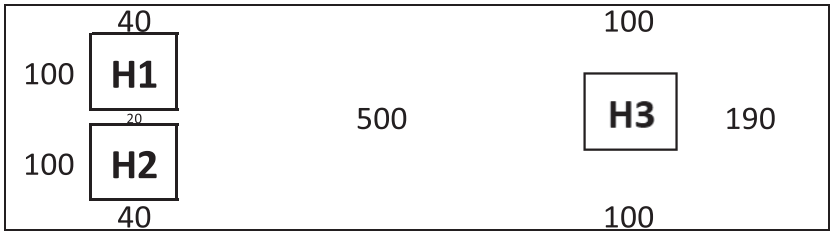

FIGURE A6 Location of cross-sections of Series H (3 cross-sections, size: 100 × 100 mm^2)

390 mm. The location of the cross-sections of plane C is visible in Figure A3; the numbering of the cross-sessions started with C1, C1, and C6 being closest to the cut plane B (see Table 2).

⇒ Series D, E and F: the distances of cross-sections from the bottom and walls of the element were 90 mm, from the top this were 80 mm, as shown by Figure A4. The locations of the three cross-sections in the length direction of the beam were:

- Series D: In the middle of the beam (distance from the same end: 1.23 m);
- Series E: At 1/3 of the length of the beam (distance from the same end: 0.82 m);
- Series F: At 1/6 of the length of the beam (distance from the same end: 0.41 m).

⇒ Series G (1.6 × 0.55 × 0.3 m^3): The dimensions of the cross-sections are 100 × 100 mm^2 and they are smaller compared to cross-sections of Series A–F; the height of this slab from the second test series was only 300 mm (Figure A5).

⇒ Series H (1.05 × 0.55 × 0.3 m^3): The same 550 mm distance was kept from the side for the cutting of plane H (Table 2). The surface of cut H was a bit curved and only three locations were considered sufficiently plain to take photographs (Figure A6)